RSC Advances

PAPER

View Article Online
View Journal | View Issue

Cite this: *RSC Adv.*, 2015, **5**, 13470

Facile synthesis of novel size-controlled antibacterial hybrid spheres using silver nanoparticles loaded with poly-dopamine spheres†

Hongyong Luo,[a] Changwei Gu,[a] Weihua Zheng,[b] Fei Dai,[a] Xinling Wang[a] and Zhen Zheng*[a]

Received 16th December 2014
Accepted 23rd December 2014

DOI: 10.1039/c4ra16469e

www.rsc.org/advances

Silver nanoparticles have been proven to exhibit excellent antimicrobial activity, but problems such as aggregation and toxicity limit their practical application. To solve these problems, a kind of sub-micrometer poly-dopamine spheres loaded with silver nanoparticles (Ag@PDS) were fabricated using a facile method. Silver nitrate was reduced by poly-dopamine spheres (PDS) without surface modification, and no other reducing agent added. This entire preparation process is very green, simple and efficient. As a result, Ag NPs have been fixed and uniformly dispersed onto the surface of the PDS, which can effectively prevent Ag NPs from aggregating or oxidizing during their application. Because the size of the uniform hybrid sphere is easily controlled by adjusting the ratio of ammonia to dopamine, it is convenient to fabricate hybrid spheres with desired sizes. These hybrids are capable of completely inhibiting bacterial growth because of their excellent antibacterial properties. Finally, the prospect of the organismal level impact of the Ag@PDS hybrid has also been proposed.

Introduction

Antibacterial materials that play critical roles in health care have always been widely studied. Silver and antibiotics, to the best of our best knowledge, are two important and popular antibacterial agents. Unfortunately, antibiotics may cause an increase in microbial drug resistance, which results in poor treatment efficacy and significant economic losses.[1] However, silver nanoparticles are proven to exhibit excellent antimicrobial activity, which is mainly due to their ability of deactivating respiratory enzymes in part by interfering with DNA replication and disrupting the cell membrane.[2] Although silver nanoparticles have been used in commercial products, they still attract the attention of researchers because of their practical applications and some elusive questions. In recent decades, the effect of the size, shape, surface charge, solution chemistry, and surface coating of silver nanoparticles on antibacterial properties has been widely studied.[3–5] However, the critical problems of aggregation and oxidation of silver nanoparticles still exist and limit their practical application because they affect the activity of silver nanoparticles.[6] To resolve these problems, several novel strategies have been employed such as the use of silver nano-composites, which can be prepared by synthesizing silver nanoparticles on the surface of nanowires, nanotubes, and nanospheres;[7–9] however, these processes are usually complex and they require surface modification of the substrate, additional reductant and multi-step processes.

Dopamine has attracted a very widespread research interest as both a hormone and neurotransmitter for many years.[10,11] Its unique property to form a coating on various bulk substrates has attracted considerable interest from researchers. Because polydopamine can be easily obtained through the self-polymerization process of dopamine under alkaline conditions, it is applied to various interfaces of different fields, such as surface modifications,[12–16] the enhancement of electronic properties,[17–20] and biological applications.[19–22] Recently, poly-dopamine spheres (PDS) have been fabricated by a facile method at room temperature.[20] PDS have many advantages such as easily controllable size, uniform spherical shape, and good thermal stability. In addition, the inherent catechol and N–H groups enable high yields of transition metal–carbon hybrid materials, which will likely enhance their application in the field of electrochemistry. The presence of these functional groups endows PDS with an active surface for absorbing and reducing metal ions. In addition, these spheres could have practical applications in the field of biomaterials because of their good biocompatibility and non-toxic properties. Due to their inherent polar groups, they can also be dispersed in many solvents; thus, they can be used as a vector for other poorly dispersible nanoparticles.

[a]*School of Chemical and Chemical Engineering, Shanghai Jiao Tong University, 800 Dongchuan Road, Minghang District, Shanghai, P. R. China. E-mail: zzheng@sjtu.edu.cn; Fax: +86 21-54741297; Tel: +86 21-54745817*

[b]*Serionix Inc., Champaign, IL, 61820, USA*

† Electronic supplementary information (ESI) available. See DOI: 10.1039/c4ra16469e

In this report, we present a novel type of uniform hybrid spheres, namely, PDS loaded with silver nanoparticles (Ag@PDS). The entire preparation process is very facile, simple and efficient; moreover, neither surface modification of PDS nor additional reductants are needed (Fig. 1). In particular, silver nitrate is directly reduced on the surface of the PDS with the assistance of sonication in ice bath. Because the size of the uniform hybrid sphere can be easily controlled by adjusting the ratio of ammonia to dopamine, it is convenient to fabricate hybrid spheres with desired sizes. In addition, PDS can efficiently disperse in many solvents, which also facilitates an efficient dispersion of Ag@PDS because of the strong bonding between silver nanoparticles and PDS. Furthermore, this strong bonding can also effectively prevent the aggregation of the silver nanoparticles and possible release of silver ions. In hybrid spheres, silver nanoparticles are uniformly distributed on the surface of PDS. This structure greatly contributes to the efficient antibacterial activity of Ag@PDS. Moreover, because Ag@PDS has characteristics of good dispersion but poor solubility in solvents, by embedding silver nanoparticles into the polymer through solution blending method, its application in the field of antibacterial material can be dramatically increased.

Furthermore, silver nanoparticles (Ag NPs) are increasingly applied in consumer products because of their antimicrobial properties, but they may have adverse effects on organisms when they enter biotic receptors, although the mechanisms of Ag NP toxicity have not been fully explained. In particular, there is debate as to whether toxicity can be directly attributed either to the nanoparticles themselves or to dissolved silver ions released from Ag NPs.[23] Liyan Yin's study shows that the release of silver in the form of nanoparticles may be of primary importance compared to the release of silver ions from NPs.[24] In our study, silver nanoparticles loaded with poly-dopamine spheres (Ag@PDS) have high antibacterial properties, and their size can be controlled from hundreds of nanometers to several micrometers, which allows a potentially great biocompatibility and possible tailored size effect for antibacterial applications in biotechnology and biomedical fields. Now we are doing a series of cytocompatibility tests about the Ag@PDS, and in future paper, we will discuss that the possibility of the hybrid applied in organisms due to the hybrid's bigger size and better biocompatibility of dopamine, which will also further illustrate the toxicity mechanism of AgNPs nanoparticles.

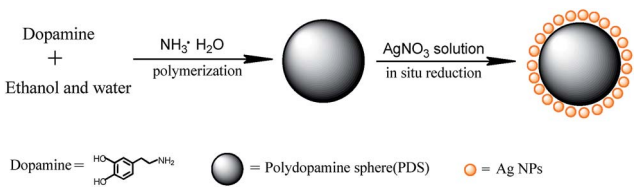

Fig. 1 Schematic illustration of the procedure for fabricating poly-dopamine sub-micrometer spheres loaded with silver nanoparticles (Ag@PDS).

Experimental

Materials

Dopamine–HCl was purchased from Aladdin-reagent Company without further treatment. Silver nitrate, ethanol and ammonia aqueous solution (25 wt%–28 wt%) were purchased from Sinopharm Chemical Reagent Co., Ltd. Phosphate buffered saline (PBS) was prepared by dissolving 7.9 g NaCl, 0.2 g KCl, 0.24 g KH_2PO_4 and 1.44 g Na_2HPO_4 in 800 ml of water. pH was adjusted to 7.40 with 1 M NaOH and 1 M HCl, and the solution was mixed with additional water to 1 L in a volumetric flask. Bacterial strains, such as *Staphylococcus aureus* (ATCC6538) and *Escherichia coli* (ATCC8739), were purchased from The Shanghai Fu Xiang Biological Technology Co., Ltd. Tryptic soy agar was obtained from The Shanghai Zhi Yan Biological Technology Co., Ltd.

Synthesis of poly-dopamine spheres (PDS)

The synthesis was similar to a previous study.[20] Deionized water (90 ml) was mixed with ethanol (40 ml) at room temperature, and aqueous solution of ammonia (NH_4OH, 1 ml, 25%) was added in the abovementioned solution with mild stirring for 30 minutes. Dopamine hydrochloride (0.5 g) was dissolved in deionized water (10 ml), and then injected into the mixture. Then, the reaction was allowed to proceed for 30 hours, and PDS were obtained by centrifugation or filtration and washed with water three times. The control over the size of the PDS was achieved by adjusting the amount of aqueous solution of ammonia.[20]

Synthesis of poly-dopamine spheres loaded with silver nanoparticles (Ag@PDS)

The obtained PDS were dispersed in deionized water with stirring and sonication for several minutes. Then, 0.8 g of silver nitrate was dissolved in deionized water (10 ml), and added dropwise into the PDS dispersion. The reduction reaction was carried out for 10 min in ice bath with the assistance of sonication. The Ag@PDS were collected by centrifugation or filtration and washed with deionized water three times. Finally, the products were dried at 60 °C in vacuum for further use.

Characterization

All the SEM patterns were acquired using a scanning electron microscope (JSM-7401F, JEOL) at an acceleration voltage of 5 kV. Energy dispersive X-ray spectroscopy (EDS) analysis was also performed on a JSM-7401F JEOL instrument during SEM. The morphology of samples was also characterized by a transmission electron microscope (TEM, JEOL, JEM-2100, with an accelerating voltage of 100 kV) equipped with an Oxford INCA Energy TEM 200 EDX system. Particle size distribution was measured using dynamic light scattering (DLS) (Zetasizer ZS, Malvern Instruments Ltd.). Fourier transform infrared spectra (FTIR) were recorded on a Perkin-Elmer 1000 FTIR spectrometer, and X-ray diffraction (XRD) data were recorded on a Rigaku D/Max 2550 (Cu Kα, $\lambda = 1.5418$ Å) with a 2θ scan configuration

in the range of 5°–90°. The surface chemical composition was analyzed using a Shimadzu-Kratos (AXIS Ultra) X-ray photoelectron spectrometer (XPS).

Bactericidal testing

Inhibition efficiency. The antimicrobial activity of the Ag@PDS was determined using inhibition efficiency, and the bactericidal experiment was carried out with the Gram-negative bacteria *Escherichia coli* and Gram-positive bacteria *Staphylococcus aureus*. Note that a modified AATCC-100 biocidal testing protocol was employed. 100 μl *E. coli* (ATCC8739) or *S. aureus* (ATCC6538) bacterial suspension was grown in a 160 ml MHB (Mueller-Hinton Broth, cation adjusted) at 37 °C for 12 h. Then, the bacteria-containing suspension was diluted 50 times to enable the separation of bacterial colonies to be distinctly visible and containing $\sim 10^6$ CFU ml^{-1} colonies. The algae filament was collected by centrifugation (5000 rpm, 10 min) from 30 ml of incubated bacterial suspension containing $\sim 10^6$ CFU ml^{-1} colonies; subsequently, 30 ml phosphate buffered saline (PBS) was added to the algae filament. Then, 0.15 mg ml^{-1} Ag@PDS, PDS, and Ag NPs suspension was added to the bacteria solution, respectively. Each measurement was repeated five times to eliminate accidental factors and get statistical results. The suspension was placed into a shaker ZHWY-2102C for another 18 h, and then 200 μl of the final solution was spread out on a plate and incubated at 37 °C for 24 h. Subsequently, the surviving bacteria on the controls and experimental plates were observed.

Zone of inhibition (ZOI). The antimicrobial activities of the Ag@PDS composite spheres were also analyzed by inhibition zone testing. For the inhibition zone test, *S. aureus* was grown in 160 ml MHB (Mueller-Hinton Broth, cation adjusted) at 37 °C for 12 h. Then, 200 μl bacterial suspension was uniformly spread over a Luria–Bertani (LB) agar plate. Samples were coated with 5 mg of Ag@PDS hybrid sphere, PDS, and Ag NPs and were carefully placed at the center of the agar plate without touching the other parts and incubated at 37 °C for 24 h. Each measurement was repeated five times to eliminate accidental factors and get statistical results. The clear zones in the center of the disks were then photographed and measured using a scale that represented the antibacterial properties of the different composites.

Results and discussion

Microstructure and morphology studies

Initially, uniform PDS were synthesized through a facile process carried out at room temperature with gentle stirring (Fig. 1). Note that this process takes 30 hours to obtain spheres with uniform shape.[20] In this study, we found that PDS were formed in the solution after only 12 hours and the size was also similar to that of the final products that were obtained after 30 hours; however, the morphology of the final spheres was much more uniform. In addition, in this synthesis process, the mild stirring plays a key role to obtain uniform spheres. Note that various sizes of PDS ranging from hundreds of nanometers to several micrometers have been successfully synthesized. However, the deterioration of dopamine, which is easily oxidized, probably results in products of slightly different size (about several to tens nanometers) at the same ratio of ammonia to dopamine under the same experimental condition.

The widespread application of poly-dopamine has also raised interest of researchers to study the mechanism of dopamine polymerization in recent years (ESI, Fig. S1†),[16] but the mechanism, to our best knowledge, has not yet been clearly demonstrated. In this work, we focus on analyzing the structure of PDS. The typical SEM and TEM images of PDS are shown in Fig. 2. From the electron microscopy images, it can be clearly seen that these organic spheres are uniform in size. Moreover, the diameter of PDS can be easily controlled by altering the ratio of ammonia to dopamine.[20] The chemical composition of the sample was determined using energy dispersive X-ray spectroscopy (SEM-EDS) (ESI, Fig. S2†). There were peaks for the elemental carbon, oxygen, nitrogen and silver in the SEM-EDS spectrum for Ag@PDS, while there were peaks for only carbon, oxygen and nitrogen in the SEM-EDS spectrum for PDS. UV-vis measurement (ESI, Fig. S3†) shows an absorbance at 280 nm. This can be attributed to catechol groups in PDS, which can reduce silver nitrate. PDS contain several polar groups, such as –OH and C–O, which facilitate a very good dispersion in many solvents. Meanwhile, many previous study about good biocompatibility of poly-dopamine provide support that PDS which is a kind of organic spheres composed by poly-dopamine probably possesses a good compatibility in organism and various biomacromolecules.

To obtain silver nanoparticles loaded on PDS as a hybrid, we mixed the PDS dispersion with silver nitrate solution in ice bath with sonication. Compared with other reduction processes, no additional reductant and heating are needed. Note that silver nitrate solution was directly reduced to silver nanoparticles because of the catechol groups in the spheres. After reduction, Ag nanoparticles are tightly bound to the surface of PDS. Thus, this strategy of obtaining the target products is very simple, facile and environmentally friendly. The TEM images in Fig. 3a–c show that the silver nanoparticles are successfully attached and uniformly dispersed on PDS. The size of the Ag nanoparticles on PDS is about 12–18 nm and their shape is spherical. This sphere-structure effectively prevents the aggregation of silver nanoparticles. The chemical composition of the sample was determined using energy dispersive X-ray spectroscopy

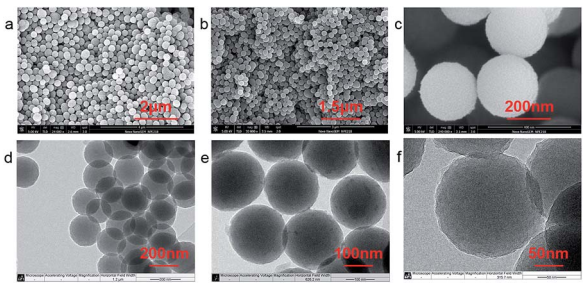

Fig. 2 SEM (a–c) and TEM (d–f) images of poly-dopamine spheres (PDS) with different scale bars.

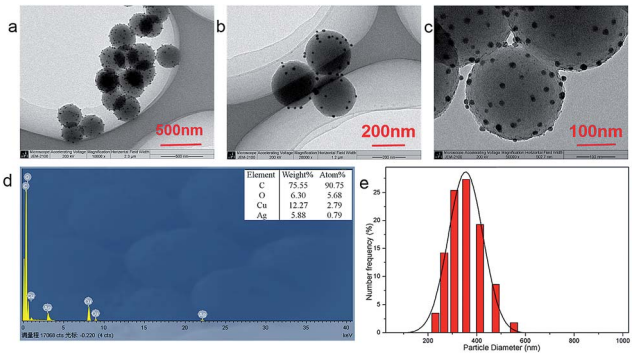

Fig. 3 TEM images (a–c) of poly-dopamine spheres loaded with silver nanoparticles (Ag@PDS) with different scale bars, and (d) EDS pattern and (e) DLS curve of Ag@PDS.

(EDS). As shown in Fig. 3d, there are several types of peaks in the EDS spectrum obtained from Ag@PDS, which correspond to the elemental carbon, oxygen, silver. It also confirms the existence of Ag NPs on the surface of the PDS. The elemental atoms results, which are in the inset table of Fig. 3d, also confirm that the particles formed on the PDS surface are composed of silver. The dynamic light scattering (DLS) result (Fig. 3e) shows that Ag@PDS are of ~350 nm with narrow size distribution, which agrees with the size measured by TEM.

Before the TEM measurement, Ag@PDS were ultrasonicated for about 30 minutes; however, silver nanoparticles were still attached on PDS and no pure particles were found. This provides evidence that the bonding between the silver nanoparticles and PDS is strong and stable. This strong bonding ensures that the nanostructure will not degrade in the process of embedding Ag@PDS into various biomacromolecules. We found that the growth speed of Ag nanoparticles on PDS is very fast with the assistance of sonication. The reaction time to obtain the abovementioned Ag nanoparticles is only 10 minutes; thus, this process is rapid and efficient.

Crystal forms of Ag@PDS

Crystal forms of the PDS and Ag@PDS can be identified with XRD patterns (Fig. 4). The XRD pattern for the obtained Ag@PDS (Fig. 4b) demonstrates the existence of PDS loaded with silver. The broad XRD reflection peak at 23.2° could be attributed to the diffraction of the amorphous structures of the PDS. Five XRD diffraction peaks of Ag@PDS at 2θ of 38.1°, 44.4°, 64.6°, 77.5° and 81.6° correspond to the diffraction of the (111), (200), (220), (311), and (222) lattice planes, indicating a face-centered-cube (FCC) phase of the Ag crystal (JCPDS file no. 04-0783). This evidently reveals that silver ions have been reduced to 0 value of metallic by PDS. Moreover, the peaks belonging to the amorphous PDS did not change, indicating that the reduction process did not affect the crystallography structure as well as the properties of PDS. The TEM, EDS and XRD results demonstrate that the AgNPs were successfully synthesized on the surface of PDS by this simple, facile reduction process.

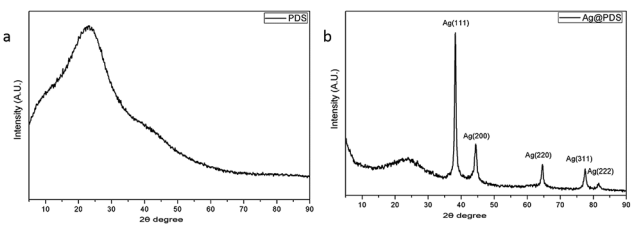

Fig. 4 XRD patterns of (a) poly-dopamine spheres (PDS) and (b) poly-dopamine spheres loaded with silver nanoparticles (Ag@PDS).

FT-IR analysis of Ag@PDS

FT-IR spectroscopy was performed to investigate the surface chemical structure of Ag@PDS as well as the binding interactions between the PDS and Ag NPs, and the spectra are illustrated in Fig. 5. The spectrum of Ag@PDS display well-defined characteristic bonds that appear in the spectrum of the PDS; however, they are slightly shifted and with different relative intensity, indicating that the reaction process did not affect the surface chemical structure as well as the properties of PDS. The absorption band at 3379 cm^{-1}, which corresponds to the stretching vibrations of –OH and N–H groups in the PDS, broadened and underwent a low-frequency shift to 3357 cm^{-1} for Ag@PDS. Such characteristics are attributed to the hydrogen bonding between PDS and Ag NPs. Moreover, the sharp peaks at 1627 cm^{-1} and 1292 cm^{-1}, which are attributed to the C=O and C–O bonds, broadened and gradually shifted to lower wavenumbers of 1608 cm^{-1} and 1268 cm^{-1}, respectively. On the other hand, the peak for C=N and C=C at 1512 cm^{-1} almost stays the same; thus, the peak shifting could be due to bond formation between silver and oxygen; moreover, the catechol and hydroxyl groups were oxidized to quinone and carbonyl group, respectively, while Ag^{+} was reduced to Ag^{0}. The interaction facilitates the attachment of Ag NPs on the surface of the PDS, leading to the steric stabilization of the particles. Furthermore, the remaining positively charged PDS could prevent the aggregation of Ag NPs by providing reciprocal electrostatic repulsion.

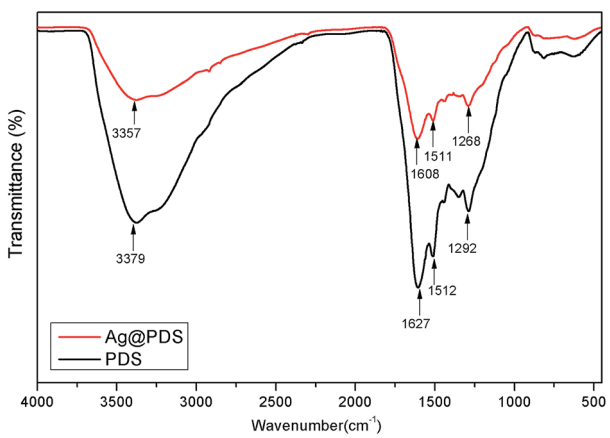

Fig. 5 FT-IR spectra of poly-dopamine spheres (PDS) and poly-dopamine spheres loaded with silver nanoparticles (Ag@PDS).

XPS study of Ag@PDS

To better understand the mechanism underlying the formation of the Ag@PDS, the results obtained were further verified by X-ray photoelectron spectroscopy (XPS) analysis to further illustrate the composition of PDS and Ag@PDS. Fig. 6 shows the XPS wide scan of the PDS and Ag@PDS, and high-resolution spectra of Ag3d, O1s and C1s. The scan survey spectra (Fig. 6a) of PDS and Ag@PDS surface showed almost the same peak components for C1s, N1s (ESI, Fig. S4†) and O1s.[25] In addition, Ag@PDS exhibited two specific peaks with binding energies of 368.0 eV and 374.0 eV in Fig. 6b, which were attributed to $Ag3d_{5/2}$ and $Ag3d_{3/2}$ electrons of Ag0, respectively. The spin energy separation was identified as 6.0 eV, which indicates that the silver on the PDS surface is metallic Ag0 in nature; in turn, this further supports the conclusion that Ag NPs have been successfully loaded on the surface of PDS. Note that the XPS binding energy of silver is somewhat lower than the values reported by Gole *et al.*[26] This may be partly caused by the bonding interaction between the Ag NPs and the surface of PDS.

Fig. 6c and d show the O1s high resolution spectrum of PDS and Ag@PDS, respectively, with both of them having two types of oxygen species. One peak at 530.5 eV is closely associated with the quinone group or carbonyl group (C═O) oxygen, whereas the other peak at 532.6 eV is attributed to the oxygen of the surface catechol groups or hydroxyl groups (–OH). The differences between the O1s spectra for the PDS and Ag@PDS are as follows: after the facile stirring process with the PDS and $AgNO_3$, the O1s peaks of the PDS at 532.6 eV and 530.5 eV shift to 532.5 eV and 530.9 eV for the Ag@PDS, respectively. The spin energy separation of Ag@PDS notably shifts to a value lower than that for PDS. In addition, the proportion of exposed O–H/C═O decreased from 24.6 (96.1%/3.9%) to 7.9 (87.9%/11.1%). These variations are due to the interactions between the silver and the oxygen-containing functional groups. Oxygen-containing functional groups are the most common functionality in activated carbons, and they can adsorb metal ions through ion-exchange reactions. Moreover, only a small amount of energy is required to readily move atomic oxygen through the silver lattice.[27,28] The interaction between the AgNPs and supporting PDS will directly lead to the strong adherence of AgNPs to the PDS surface, which is very useful and essential for practical applications.

The C1s high-resolution spectrum of the PDS (Fig. 6e) could be curve-fitted with four peak components, having binding energies at 284.2 eV for the sp2C species, at 285.0 eV for the sp3C species, at 286.0 eV for the C–O species, and at 287.7 eV for the C–N species. The C1s core-level spectrum of the Ag@PDS (Fig. 6f) has almost the same peak components as that of the PDS but the peaks are shifted to 284.5 eV, 285.3 eV, 286.1 eV, and 288.1 eV, respectively. The peak for the C–O species is substantially decreased, which shows that many oxygen-containing functional groups have reacted or been removed due to the interaction of catechol groups with silver.

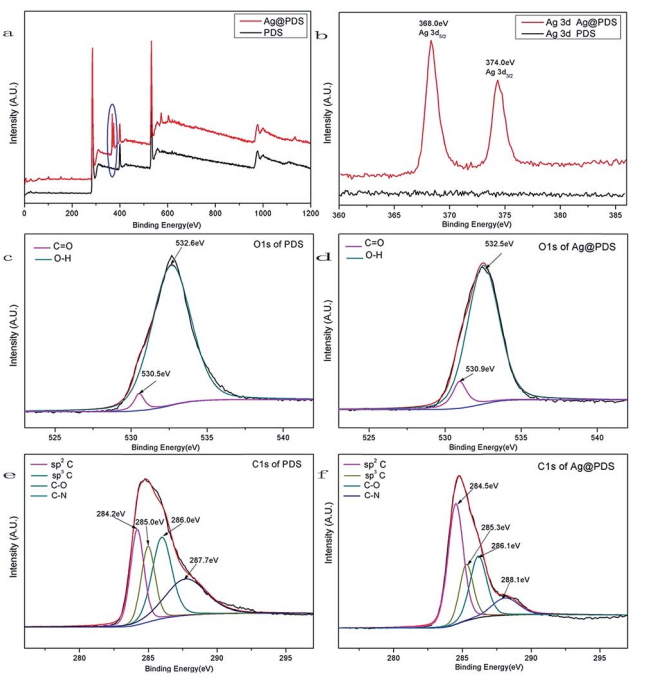

Fig. 6 X-ray photoelectron spectra (XPS) of (a) scan survey, (b) Ag3d, (c and d) O1s, (e and f) C1s of poly-dopamine spheres (PDS) and poly-dopamine spheres loaded with silver nanoparticles (Ag@PDS).

Thermogravimetric analysis of Ag@PDS

Thermogravimetric analysis (TGA) was carried out within the temperature range of 40–800 °C to examine the thermal stability of PDS and Ag@PDS. As expected, both PDS and Ag@PDS show excellent thermal stability; moreover, 51.6% and 52.5% residual weight of PDS and Ag@PDS, respectively, was observed even at the end of the analysis (800 °C) under a N_2 atmosphere, and they exhibit almost the same behavior in Fig. 7. The difference of the TGA curve can be found under an air atmosphere, while Ag@PDS show a relatively slower rate of weight loss, and it reached balance at 625 °C with 6.41% residual weight; however, the PDS reached balance at a higher temperature of 700 °C with 3.06% residual weight.

Solubility measurement

For the feasibility of practical applications, the solubility and dispersibility of Ag@PDS have been studied (Fig. 8). This experiment demonstrated that several common solvents, such as water, acetone, 1,4-dioxane, chloroform, toluene, and *N*,*N*-dimethylformamide (DMF), are unable to dissolve these spheres. However, due to the inherent polar group, the Ag@PDS

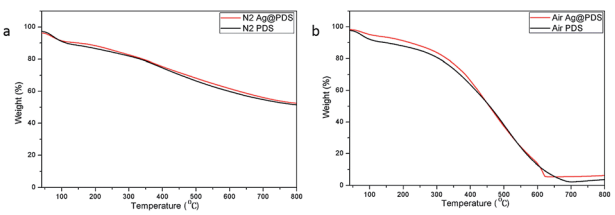

Fig. 7 TGA curves of (a) poly-dopamine spheres (PDS) and (b) poly-dopamine spheres loaded with silver nanoparticles (Ag@PDS).

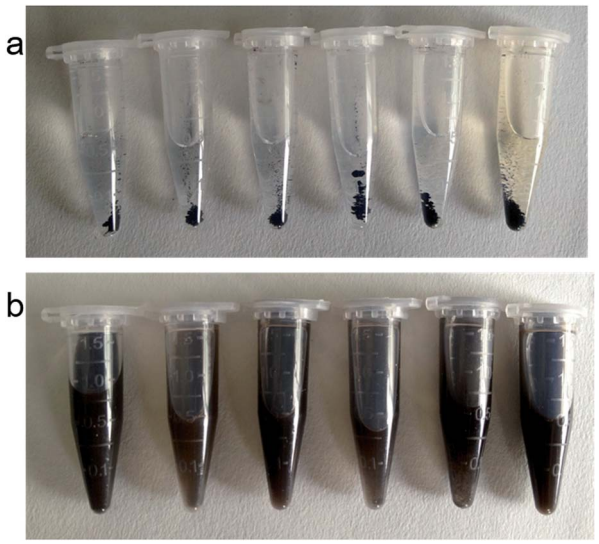

Fig. 8 Images of solubility (a) and dispersion (b) measurement of poly-dopamine spheres loaded with silver nanoparticles (Ag@PDS) in various solvents. The solvents are water, acetone, 1,4-dioxane, chloroform, toluene, and DMF (from left to right).

can be dispersed in these solvents after ultrasonication. This characteristic of good dispersion but poor solubility of the spheres make them perfect vectors for Ag nanoparticles, which will result in the uniform and stable dispersion of Ag nanoparticles in the composite through the important method of solution blending.

Antibacterial property

Samples designated as $Ag@PDS_{1.0}$, $Ag@PDS_{1.25}$, $Ag@PDS_{1.5}$, $Ag@PDS_{1.75}$ and $Ag@PDS_{2.0}$ were achieved by adjusting the amount of aqueous solution of ammonia to 1.0 ml, 1.25 ml, 1.5 ml, 1.75 ml and 2.0 ml and keeping the amount of dopamine hydrochloride the same (0.5 g). TEM images (Fig. 9) show that different sizes of the uniform PDS were obtained by adding different amount of ammonia aqueous solution. The diameter of the PDS in $Ag@PDS_{1.0}$, $Ag@PDS_{1.25}$, $Ag@PDS_{1.5}$, $Ag@PDS_{1.75}$ and $Ag@PDS_{2.0}$ is 350 nm, 310 nm, 280 nm, 260 nm and 230 nm, respectively, while the that of Ag NPs in these samples is almost the same, mainly 12–18 nm. Ag content measured by TGA is 3.35%, 4.43%, 3.85%, 3.86% and 4.01% for $Ag@PDS_{1.0}$, $Ag@PDS_{1.25}$, $Ag@PDS_{1.5}$, $Ag@PDS_{1.75}$ and $Ag@PDS_{2.0}$, respectively. Pure Ag NPs were synthesized according to a previously reported method,[29] and their size was similar to that of Ag NPs on the surface of PDS in Ag@PDS.

To investigate the antibacterial activity of our new hybrid material, the bactericidal experiment was carried out with the Gram-negative bacteria *E. coli* and Gram-positive *S. aureus*. After PDS were dispersed, the color of the LB medium became dark; thus, it was impossible to observe the turbidity of the LB medium. Therefore, in this report, the antibacterial efficacy of Ag@PDS was evaluated by the inhibition rate experiment on LB-agar plates. After the LB-agar plates solidified, the bacterial suspension was spread on the LB-agar plates. Then, the LB-agar plates were cultured at 37 °C for 24 h, and there was a robust growth of *E. coli* bacteria with no samples added in Fig. 10a. No considerable antibacterial activity was observed in the disk with PDS (Fig. 10b), indicating that PDS were not toxic to the bacteria. In addition, another controlled experiment, in which the suspension consisted of *E. coli* and $Ag@PDS_{2.0}$ was carried out under the same condition. Fig. 10c shows that very few bacteria were observed and this strain is inhibited, which indicates that this new hybrid material has very strong antimicrobial activity for *E. coli*. In addition, from Fig. 11, residual bacteria decrease with the size of Ag@PDS. $Ag@PDS_{1.75}$ and $Ag@PDS_{2.0}$ even exhibit full inhibition of *S. aureus*, and the minimum inhibitory concentration (MIC) against *S. aureus* of $Ag@PDS_{2.0}$ is 6 μg ml^{-1} of Ag, which is comparable that of pure Ag NPs. This suggests that the Ag@PDS nanohybrid is an efficient antibacterial material for both Gram-negative and Gram-positive bacteria. Moreover, the excellent antimicrobial activity has a close relationship with the novel nano-structure, which can prevent the agglomeration of the silver nanoparticles, and the large surface area of PDS also provides high load capacity for silver nanoparticles with the assistance of its functional groups.

To further check the antibacterial effect of Ag@PDS, the Gram-positive bacteria, *S. aureus*, was chosen using the zone of inhibition (ZOI) in a disk diffusion test. The ZOI reflected the

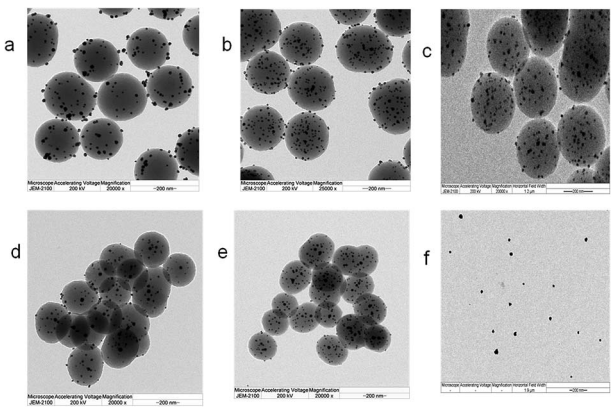

Fig. 9 TEM images, with 200 nm scale bar, of different sizes of poly-dopamine spheres loaded with silver nanoparticles (Ag@PDS) controlled by adjusting the amount of aqueous ammonia: (a) 1.0 ml, (b) 1.25 ml, (c) 1.5 ml, (d) 1.75 ml, (e) 2.0 ml and (f) pure Ag NPs. Ag@PDS of different sizes are applied in the antibacterial experiments.

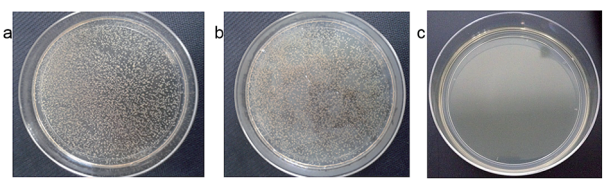

Fig. 10 Images of LB-agar plates used in the antibacterial experiments of samples against *E. coli*: (a) control, (b) poly-dopamine spheres (PDS), and (c) poly-dopamine spheres loaded with silver nanoparticles (Ag@PDS).

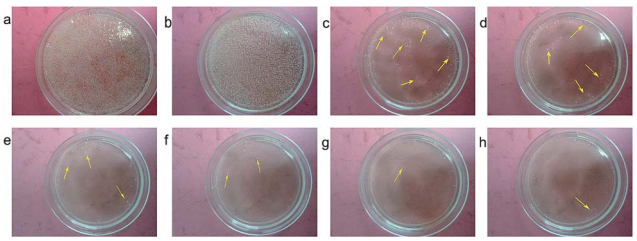

Fig. 11 Antibacterial efficacy of samples against *S. aureus*. There is a robust growth of bacteria in images (a) and (b), while there are only a few surviving bacteria in (c)–(h). Samples: (a) control, (b) PDS, (h) pure Ag NPs, (c)–(g) Ag@PDS*x* with different amounts of aqueous ammonia: (c) $x = 1.0$ ml; (d) $x = 1.25$ ml; (e) $x = 1.5$ ml; (f) $x = 1.75$ ml; (g) $x = 2.0$ ml.

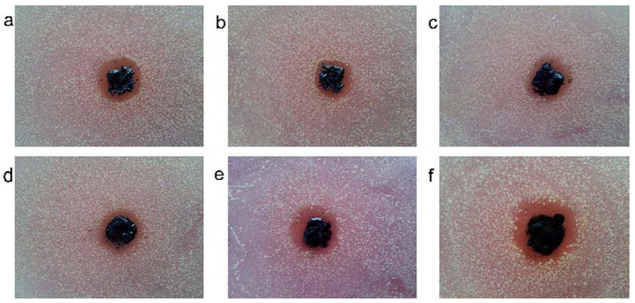

Fig. 12 Disk diffusion tests for different samples against *S. aureus*. The zones of inhibition (ZOI) appear with an obvious circle, indicating a noticeable antibacterial effect. (a) Pure Ag NPs, (b)–(f) Ag@PDS with different amounts of aqueous ammonia: (b) $x = 1.0$ ml; (c) $x = 1.25$ ml; (d) $x = 1.5$ ml; (e) $x = 1.75$ ml; (f) $x = 2.0$ ml.

magnitude of the susceptibility to the bacteria. In Fig. 12, it can be seen that clear and significant zones formed against the growth of *S. aureus* in disks with the Ag NPs and Ag@PDS hybrid, and the corresponding zones of inhibition (ZOI) are listed in Table 1.

It can be seen that the average ZOI values (ratio of ZOI diameter to sample diameter) for the Ag NPs with *S. aureus* was 1.81 ± 0.31, while the values for Ag@PDS$_{1.0}$, Ag@PDS$_{1.25}$, Ag@PDS$_{1.5}$, Ag@PDS$_{1.75}$ and Ag@PDS$_{2.0}$ are 1.51 ± 0.33, 1.72 ± 0.25, 1.75 ± 0.40, 1.83 ± 0.27 and 1.94 ± 0.33, respectively. After the normalization of the Ag concentration to 200 μg, the normalized ZOI values of Ag@PDS$_{1.0}$, Ag@PDS$_{1.25}$, Ag@PDS$_{1.5}$, Ag@PDS$_{1.75}$ and Ag@PDS$_{2.0}$ are 1.61 ± 0.39, 1.65 ± 0.23, 1.78 ± 0.42, 1.86 ± 0.28 and 1.94 ± 0.33, respectively. The specific surface area $s/m = 4\pi r^2/(\rho 4/3\pi r^3) = 3/(\rho r)$ (unit, $m^2\ g^{-1}$) is inversely proportional to the particle size with the same density. This indicates that smaller Ag@PDS have a larger specific surface area, which contributes to better antibacterial activity.

The normalized ZOI value of Ag NPs at normalized Ag content (200 μg) is 1.03 ± 0.01, which is very unreasonable because Ag NPs have excellent antibacterial activity. According to a study,[30] the antibacterial activity of Ag NPs increases with the increasing concentration until a maximum value has been reached, and then the antibacterial activity stays the same even with the further addition of Ag NPs to some point (extreme point). The maximum value and the extreme point is limited by the size of Ag NPs, specifically smaller Ag NPs have a higher maximum value and higher extreme point partly due to its larger specific surface area (s/m). Thus, the most probable explanation is that the normalized ZOI value for Ag NPs at normalized Ag content (200 μg) is the maximum value of 1.81 ± 0.31, and it remains unchanged with the further addition of Ag NPs up to 5000 μg. Based on these antibacterial results, we draw the conclusion that the Ag@PDS composites, especially small sized Ag@PDS, have better antibacterial properties in comparison with those of the pure Ag NPs.

According to a previous study, the influence of the antibacterial efficiency of Ag NPs might have been derived from the fact that dispersed Ag NPs tend to aggregate and separate from solutions.[6] In our work, Ag NPs have been fixed and uniformly dispersed onto the surface of the PDS, which can effectively prevent the aggregation and oxidation of Ag NPs during their application. In addition, the XPS and FTIR results for the Ag@PDS show surface functional groups, such as C–O and O–H, which can significantly improve the capacity and dispersion ability of the Ag@PDS. Consequently, the Ag@PDS composites can bind and remain in close proximity to the bacterial surface and efficiently inhibit bacterial growth. Therefore, these composites are highly efficient inhibitors of bacterial growth.

Conclusion

We presented a novel micro-structure, which is composed of uniform PDS and Ag nanoparticles. PDS as a carrier in this structure effectively prevents the agglomeration of Ag nanoparticles; moreover, its antibacterial activity has been studied for the first time in this study. The entire preparation process is

Table 1 ZOI value (ratio of ZOI diameter to sample diameter) of samples against *S. aureus*

Samples	Ag content (μg)	ZOI value (mm mm^{-1})	normalized Ag content (μg)	normalized ZOI value (mm mm^{-1})
PDS	0	—	0	—
Ag NPs	5000	1.81 ± 0.31	200	1.81 ± 0.31
Ag@PDS$_{1.0}$	167.5	1.51 ± 0.33	200	1.61 ± 0.39
Ag@PDS$_{1.25}$	221.5	1.72 ± 0.25	200	1.65 ± 0.23
Ag@PDS$_{1.5}$	192.5	1.75 ± 0.40	200	1.78 ± 0.42
Ag@PDS$_{1.75}$	193	1.83 ± 0.27	200	1.86 ± 0.28
Ag@PDS$_{2.0}$	200.5	1.94 ± 0.33	200	1.94 ± 0.33

very facile, simple, green and efficient; moreover, neither surface modification of PDS nor additional reductants are needed. In the hybrid sphere, silver nanoparticles are uniformly distributed on the surface of PDS, which effectively prevents the aggregation of the silver nanoparticles; moreover, this hybrid material has high antibacterial activity. Because of the PDS's good compatibility with the substrates, it greatly contributes to the stable and uniform distribution of silver nanoparticles in various media. This will dramatically increase the antibacterial application of this hybrid sphere in biotechnology and biomedical fields. In addition, our hybrid of silver nanoparticles loaded on poly-dopamine spheres has high antibacterial property and possesses controllable sizes ranging from hundreds of nanometers to several micrometers, which makes its application in biomedical fields possible for reducing the toxicity of Ag NPs, and further provides some support to illustrate the toxicity mechanism of Ag nanoparticles.

Acknowledgements

This project was supported by the National Science Fund of China (20974061) and the Shanghai Leading Academic Discipline Project (no. B202). We thank Dr Limin Sun from Instrumental Analysis Center of Shanghai Jiao Tong University for his assistance in the XPS experiments.

Notes and references

1 J. Tang, Q. Chen, L. G. Xu, S. Zhang, L. Z. Feng, L. Cheng, H. Xu, Z. Liu and R. Peng, *ACS Appl. Mater. Interface*, 2013, **5**, 3867–3874.
2 J. S. Lee and W. L. Murphy, *Adv. Mater.*, 2013, **8**, 1173–1179.
3 Z. M. Xiu, Q. B. Zhang, H. L. Puppala, V. L. Colvin and P. J. J. Alvarez, *Nano Lett.*, 2012, **12**, 4271–4275.
4 C. Carlson, S. M. Hussain, A. M. Schrand, L. K. Braydich-Stolle, K. L. Hess, R. L. Jones and J. J. Schlager, *J. Phys. Chem. B*, 2008, 112–117.
5 X. Y. Yang, A. P. Gondikas, S. M. Marinakos, M. Auffan, J. Liu, H. Hsu-Kim and J. N. Meyer, *Environ. Sci. Technol.*, 2012, **46**(2), 1119–1127.
6 Z. Zhang, J. Zhang, B. Zhang and J. Tang, *Nanoscale*, 2013, **5**, 118–123.
7 M. Lv, S. Su, Y. He, Q. Huang, W. B. Hu, D. Li, C. H. Fan and S. T. Lee, *Adv. Mater.*, 2010, **22**, 5463–5467.
8 P. Gunawan, C. Guan, X. H. Song, Q. Y. Zhang, S. S. J. Leong, C. Y. Tang, Y. Chen, M. B. Chan-Park, M. W. Chang, K. A. Wang and R. Xu, *ACS Nano*, 2011, **5**, 10033–10040.
9 J. H. Cui, C. F. Hu, Y. H. Yang, Y. J. Wu, L. F. Yang, Y. L. Wang, Y. L. Liu and Z. Y. Jiang, *J. Mater. Chem.*, 2012, **22**, 8121–8126.
10 R. M. Wightman, L. J. May and A. C. Michael, *Anal. Chem.*, 1988, **60**, 769–775.
11 A. Zhang, J. L. Neumeyer and R. J. Baldessarini, *Chem. Rev.*, 2007, **107**, 274–278.
12 L. Wang, D. Wang, Z. H. Dong, F. X. Zhang and J. Jin, *Nano Lett.*, 2013, **13**(4), 1711–1716.
13 J. H. Kong, W. A. Yee, L. P. Yang, Y. F. Wei, S. L. Phua, H. G. Ong, J. M. Ang, X. Li and X. H. Lu, *Chem. Commun.*, 2012, **48**, 10316–10318.
14 H. Jiang, L. P. Yang, C. Z. Li, C. Y. Yan, P. S. Lee and J. Ma, *Energy Environ. Sci.*, 2011, **4**, 1813–1821.
15 M. H. Ryou, Y. M. Lee, J. K. Park and J. W. Choi, *Advanced Materials*, 2011, **27**, 3066–3070.
16 N. F. D. Vecchia, R. Avolio, M. Alfè, M. E. Errico, A. Napolitano and M. d'Ischia, *Adv. Funct. Mater.*, 2013, **23**, 1331–1340.
17 S. M. Kang, I. You, W. K. Cho, H. K. Shon, T. G. Lee, I. S. Choi, J. M. Karp and H. Lee., *Angew. Chem., Int. Ed.*, 2010, **49**, 9401–9404.
18 S. L. Phua, L. Yang, C. L. Toh, G. Q. Du, S. K. Lau, A. Dasari and X. Lu, *ACS Appl. Mater. Interfaces*, 2013, **5**, 1302–1309.
19 D. E. Fullenkamp, J. G. Rivera, Y. K. Gong, K. H. Lau, L. He, R. Varshney and P. B. Messersmith, *Biomaterials*, 2012, **33**, 3783–3791.
20 K. Ai, Y. L. Liu, C. P. Ruan, L. H. Lu and G. Q. Lu, *Adv. Mater.*, 2013, **7**, 998–1003.
21 L. Zhang, J. J. Wu, Y. X. Wang, Y. H. Long, N. Zhao and J. Xu, *J. Am. Chem. Soc.*, 2012, **134**, 9879–9881.
22 J. W. Cui, Y. J. Wang, A. Postma, J. C. Hao, L. H. Rigau and F. Caruso, *Adv. Funct. Mater.*, 2010, **10**, 1625–1631.
23 C. M. Jones and M. V. Eric Hoek, *J. Nanopart. Res.*, 2010, **12**, 1531–1551.
24 L. Y. Yin, Y. W. Cheng, B. Espinasse, B. P. Colman, M. Auffan, M. Wiesner, J. Rose, J. Liu and E. S. Bernhardt, *Environ. Sci. Technol.*, 2011, **45**, 2360–2367.
25 J. F. Moulder, W. F. Stickle, P. E. Sobol and K. D. Bomben, *Handbook of X-ray Photo electronspectroscopy: A reference Book of Standard Spectra for identification and Interpretation of XPS Data*, Physical Electronics, Reissue edition, USA 18725, Lakedrive East, Chanhassen, MN 55317, 1992.
26 A. Gole, S. R. Sainkar and M. Sastry, *Chem. Mater.*, 2000, **12**, 1234–1239.
27 R. A. Outlaw and M. R. Davidson, *J. Vac. Sci. Technol., A*, 1994, **12**, 854–860.
28 M. E. Eberhart, M. M. Donovan and R. A. Outlaw, *Phys. Rev. B: Condens. Matter*, 1992, **46**, 12744–12747.
29 J. H. Cui, C. F. Hu, Y. H. Yang, Y. J. Wu, L. F. Yang, Y. L. Wang, Y. L. Liu and Z. Y. Jiang, *J. Mater. Chem.*, 2012, **22**, 8121–8126.
30 S. Agnihotri, S. Mukherjin and S. Mukherj, *RSC Adv.*, 2014, **4**, 3974–3983.